Self-adjoint integral operator for bounded nonlocal transport

J. E. Maggs and G. J. Morales

Department of Physics and Astronomy, University of California, Los Angeles, California 90095, USA

An integral operator is developed to describe nonlocal transport in a one-dimensional system bounded on both ends by material walls. The "jump" distributions associated with nonlocal transport are taken to be Lévy α-stable distributions, which become naturally truncated by the bounding walls. The truncation process results in the operator containing a self-consistent, convective inward transport term (pinch). The properties of the integral operator as functions of the Lévy distribution parameter set $[\alpha, \gamma]$ and the wall conductivity are presented. The integral operator continuously recovers the features of local transport when $\alpha = 2$. The self-adjoint formulation allows for an accurate description of spatial variation in the Lévy parameters in the nonlocal system. Spatial variation in the Lévy parameters is shown to result in internally generated flows. Examples of cold-pulse propagation in nonlocal systems illustrate the capabilities of the methodology.

I. INTRODUCTION

Currently there is considerable interest in the study and manipulation of physical systems in which nonlocal transport (i.e., not described by Fick's law) occurs between confining walls or boundaries. Examples of recent experimental efforts in this area include studies of heat transport in semiconductor alloys [1], relaxation of photoexcited electrons in graphene [2,3], and measurements of the nondiffusive thermal conductivity in crystalline silicon [4]. In addition, there is a long history of nonlocal transport processes observed in magnetically confined plasmas surrounded by metallic walls [5–9]. The cause of nonlocal transport is often related to underlying dynamical processes in which relatively large displacements or "steps" develop, and whose statistics are non-Gaussian. By "large" it is understood to be relative to the spatial extent of the system. A convenient and frequent choice for probability distribution functions (pdfs), that can describe important transport properties in such situations, is the class of Lévy α-stable distributions. Although such distributions have intrinsic features (nonfinite moments and infinite jumps) that are obviously not physically permissible, they capture essential features of experimental relevance, as has been well documented in detailed measurements of Lévy flights of light [10].

In implementing a practical mathematical procedure to describe finite-size experiments based on a Lévy α-stable pdf, some difficult issues need to be overcome. They are related to the infinite extent of the jumps, as is extensively discussed in the review by Zaburdaev *et al.* [11], and to the interaction with the boundaries [12,13]. One approach to handling the infinite extent of the jumps is to introduce a sharp truncation of the pdf at a specified cutoff [14]. Another method [15] is to introduce an exponential tempering of the spatial fractional derivatives used in a fractional Fokker-Planck equation. Recently, Vermeersch *et al.* [16] applied the exponential tempering directly on the Lévy pdf to implement a continuous time random walk model (CTRW) [17–20] of thermoreflectance measurements.

The issue of a proper description of the coupling of the nonlocal system to an external world through a boundary involves the difficulties intrinsic to the infinite jumps, but there are other subtleties. An approach based on the fractional Fokker-Planck

description is to postulate a "sheath" or insulating layer whose dimension has to be judiciously chosen [21]. Another methodology, proposed by Zoia *et al.* [22], is to discretize the fractional Laplacian operator and solve an eigenvalue problem for free and absorbing boundaries, and in principle, to represent the solutions as a superposition of the eigenmodes. Diffusion in an open Lévy system, with a legislated reflection coefficient, has been explored by Lepri and Politi [23].

Another element for a successful modeling of a nonlocal transport experiment using Lévy pdfs is the capability to handle spatial variations in the parameters associated with the distributions. This situation may arise in physical systems because the internal dynamics switches character within various regions of the system, as has been found in some model comparisons [24]. Fractional diffusion in a composite medium has been addressed by Stickler and Schachinger using a finite-width boundary between layers of different fractional order [25].

The manuscript is organized as follows. The form of the integral operator is presented in Sec. II. Section III outlines the concepts behind the construction of the matrix operator, with the essential details for implementing numerical calculations presented in Appendix C. Section IV uses numerical studies to illustrate parameter dependencies in the steady-state case. Section V gives the results from a time-dependent system, following the effects of a cold pulse introduced into various nonlocal configurations. Section VI discusses results and presents conclusions. Subtle issues regarding the choice of grid size are explored in Appendix A, with the limit of classical transport ($\alpha = 2$) treated as a special case in Appendix B. Appendix D contains a discussion of profile scaling with the ratio of distribution width to calculation grid size, γ/h.

II. TRANSPORT EQUATION

It is desired to compute the spatial profile resulting from nonlocal transport of some scalar quantity (e.g., density or temperature) in a one-dimensional (1D) system. Transport is presumed to arise from physical entities (e.g., particles) that experience a change or "jump" from one spatial location to another. The Markovian master equation describing the probability of a "particle" being at position $\bar{x}$ at time

$\bar{t}, P(\bar{x}, \bar{t})$, is

$$\frac{\partial}{\partial \bar{t}} P(\bar{x}, \bar{t}) = -\frac{1}{\tau} \left\{ \int_{-\infty}^{\infty} d\bar{x}' \eta(\bar{x} - \bar{x}') P(\bar{x}', \bar{t}) \right.$$
$$\left. - \int_{-\infty}^{\infty} d\bar{x}' \eta(\bar{x}' - \bar{x}) P(\bar{x}, \bar{t}) \right\}$$
$$= \frac{1}{\tau} \left\{ \int_{-\infty}^{\infty} d\bar{x}' \eta(\bar{x} - \bar{x}') P(\bar{x}', \bar{t}) - P(\bar{x}, \bar{t}) \right\}. \quad (1)$$

The quantities $\bar{x}$, $\bar{t}$ are spatial position and time measured in physical units (e.g., meters and seconds). The probability of a particle having moved in the time interval $[0, \bar{t}]$ is $\psi(\bar{t})d\bar{t}$ and the probability of a particle jumping a distance $|\bar{x} - \bar{x}'|$ from $\bar{x}'$ to $\bar{x}$ is $\eta(\bar{x} - \bar{x}')d\bar{x}'$. The waiting time probability, $\psi(\bar{t})$, is assumed to be independent of position and the jump probability, $\eta(\bar{x})$, is assumed to be independent of time. The initial condition is taken to be that all the particles are located at $\bar{x} = 0$.

The pdf governing the displacement of particles is characterized by a set of parameters, $[p]$, and thus the notation in Eq. (1) is expanded to $\eta(\bar{x}) \to \eta([p], \bar{x})$. The basic form of the jump distribution, $\eta([p], \bar{x})$, is presumed to be peaked at $\bar{x} = 0$. Its Fourier transform is written as $\tilde{\eta}\{[p(0)], \bar{k}\}$, with $[p(0)]$ denoting the parameter values of the jump distribution with a peak located at $\bar{x}_p = 0$. In constructing the transport matrix presented next, the jump-distribution peak is required to be at the spatial location $\bar{x} = \bar{x}_p$. In the process of inverting the Fourier transform, the peak of the pdf can be moved to the location $\bar{x} = \bar{x}_p$ by multiplying the Fourier transform $\tilde{\eta}\{[p(0)], \bar{k}\}$ by $\exp(-i\bar{k}\bar{x}_p)$. Also, the parameter values characterizing the jump distribution with the peak located at $\bar{x} = \bar{x}_p$ can be chosen to have the values $[p(\bar{x}_p)]$. Inverting this modified Fourier transform, $\tilde{\eta}\{[p(\bar{x}_p)], \bar{k}\} \exp(-i\bar{k}\bar{x}_p)$, to obtain the spatial form of the jump distribution with peak at $\bar{x} = \bar{x}_p$, then gives a jump distribution with the spatial form $\eta[p(\bar{x}_p), \bar{x} - \bar{x}_p]$. Thus, the parameter dependence of the Fourier transform is thought of as a function of the peak location $\bar{x}_p$. Particles jumping from the location $\bar{x}_p$ to $\bar{x}$ have a jump pdf whose parameters are determined at the spatial point corresponding to the distribution peak $\bar{x}_p$. This concept is analogous to the Wentzel-Kramers-Brillouin (WKB) formalism used in the study of wave propagation through nonuniform media.

Solutions to Eq. (1) are computed, in this study, at $N + 1$ evenly spaced, discrete points, $\bar{x}_i$. In a discrete space, it is convenient to introduce an expression for the transported scalar in terms of individual probabilities, $T(\bar{x}, \bar{t}) = \sum_1^N A_i P_i(\bar{x}, \bar{t})$, where each $P_i(\bar{x}, \bar{t})$ satisfies Eq. (1) with the initial condition $P_i(\bar{x}, 0) = \delta(\bar{x} - \bar{x}_i)$. The relevant equation becomes

$$\frac{\partial}{\partial \bar{t}} T(\bar{x}, \bar{t}) - \frac{1}{\tau} \left\{ \int_{-\infty}^{\infty} d\bar{x}' \eta(\bar{x} - \bar{x}') T(\bar{x}', \bar{t}) - T(\bar{x}', \bar{t}) \right\}$$
$$= G_S(\bar{x}, \bar{t}), \quad (2)$$

where a source term $G_S(\bar{x}, \bar{t})$ has been added. Physically, if T is identified with "temperature," this source represents the external heating power density applied to a system whose internal dynamics is nonlocal.

It is desired to describe a nonlocal system of finite size, so the next assumption is that the jump distributions are nonzero

only over a limited interval. That is, the jump distributions are assumed to have zero value outside the interval $[0, L]$. The "truncation" of the jump distributions is accomplished by multiplying them by a "top hat" function,

$$f_{th}(\bar{x}) = \begin{bmatrix} 1 & \bar{x} \in [0, L] \\ 0 & \bar{x} < 0; \ \bar{x} > L \end{bmatrix}. \quad (3)$$

Since the jump distributions are probability densities, it is required that the spatial integral of the distribution is unity. For example, at constant $\bar{x}'$,

$$\int_{-\infty}^{\infty} d\bar{x} \eta[p(\bar{x}'), \bar{x} - \bar{x}'] f_{th}(\bar{x})$$
$$= \int_0^L d\bar{x} \eta[p(\bar{x}'), \bar{x} - \bar{x}'] = 1, \quad \forall \bar{x}' \in [0, L]. \quad (4)$$

Normalizing the position vector to $x = \bar{x}/L$, and the time to $t = \bar{t}/\tau$, yields the model transport equation for $T(x, t)$,

$$\frac{\partial}{\partial t} T(x, t) - \left\{ \int_0^1 dx' \eta'[p(x'), x - x'] T(x', t) - T(x, t) \right\}$$
$$= \tau G_S(x, t); \ x \in [0, 1], \quad (5)$$

where $\eta' = L\eta$ denotes the dimensionless jump distribution.

The steady-state case, in which the time derivative in Eq. (5) is zero, is useful for discussing the details of the integral operator,

$$-\int_0^1 dx' \eta'[p(x'), x - x'] T(x') + T(x) = \tau G_S(x) = S(x). \quad (6)$$

The integral in Eq. (6) represents the processes of particles jumping from all points x' in the system ($0 \leqslant x' \leqslant 1$) to a particular spatial location, $x \in [0, 1]$. The second term (the identity) represents the process of particles jumping from x to other system points x', and the identity indicates that they are certain to do this as indicated by Eq. (4). In the absence of a source ($S = 0$) these two processes need to balance each other. In Eq. (6) the source term $S(x)$ is treated as a function that is chosen by an external agent, and, in that sense, is arbitrary. The coefficients A_i in the definition of $T(x,t)$ can be found in terms of the source term, but they are not needed to proceed from Eq. (6) and thus are not computed.

The integral operator in Eq. (6) can be represented, in a discrete system, by matrix multiplication. For example,

$$\int_0^1 dx' \eta'[p(x'), x - x'] T(x') \approx \sum_j m_{ij} T_j;$$
$$m_{ij} = h \eta'[p(x_j), x_i - x_j]. \quad (7)$$

The term m_{ij} is a component of a row vector representing the jump distribution, $\eta'[p(x_j), x_i - x_j]$, and h is the grid spacing, $h = x_{n+1} - x_n = 1/N$, with $N + 1$ the number of grid points. T_j is the jth element of the column vector representing the profile $T(x)$ at the point x_j, $T_j = T(x_j)$. The second term on the left-hand side of Eq. (6) is obtained from a term similar to Eq. (7), but the column number is constant and the row number varies, $\sum_i m_{ij} T_j = T_j$ (the sum is over i rather than j), with the identity following from Eq. (4). The ith row of the second term in Eq. (6) therefore has the form δ_{ij}, that is zero for all elements except the diagonal element. The left-hand

side of Eq. (6) can thus be represented at all values $x_i \in [0, 1]$ by a square matrix operator with elements

$$M'_{ij} = \delta_{ij} - m_{ij}. \qquad (8)$$

By construction, in the absence of a source term, $S = 0$, the sum of the columns of $\boldsymbol{M}'$, $\sum_i M'_{ij} = 0$, $\forall j$, so that, for the matrix columns, the requirement of particle conservation is fulfilled. However, even for constant parameter values for the jump pdf, the ith row of the $\boldsymbol{m}$ matrix is not the same as the ith column, because of the truncation process. Therefore, for both spatially uniform and nonuniform parameter values, the conservation relationship does not hold for every row and column unless the matrix operator is made self-adjoint and the columns of the $\boldsymbol{m}$ matrix are then renormalized so that their sum is unity. For a self-adjoint transport matrix, the requirement that the spatial integral (sum) of each column of the operator is zero when the source is zero, then assures that the spatial integral of the rows is zero as well. With the integral operator expressed as a matrix operator, Eq. (5) becomes

$$\frac{\partial}{\partial t}\boldsymbol{T}_{\text{col}}(t) + \boldsymbol{M}'\boldsymbol{T}_{\text{col}}(t) = \boldsymbol{S}_{\text{col}}(t). \qquad (9)$$

The variables in Eq. (9) are normalized time, $t = \bar{t}/\tau$, and position, $x = \bar{x}/L$. The notation $\boldsymbol{T}_{\text{col}}$ indicates that the variable $T(x)$ is represented as a column vector, and $\boldsymbol{S}_{\text{col}}(t)$ is the source column vector. A description of the procedures used to make the $\boldsymbol{M}'$ operator self-adjoint is presented in Sec. III.

The present study focuses on effects associated with Lévy α-stable distributions characterized by two parameters, $p(x) = [\alpha(x), \gamma(x)]$, with alpha the order of the distribution, $1 \leqslant \alpha \leqslant 2$, and gamma the width of the distribution, $0 < \gamma$. The spatial form of the general Lévy α-stable distribution, L_{pdf}, is computed numerically, using the standard fft (fast Fourier transform) algorithm, from L_{cf}, the Lévy α-stable characteristic function [26] modified as described in the paragraph following Eq. (1),

$$L_{cf}\{[\alpha(x_p), \gamma(x_p)], k\} = \exp[-|\gamma(x_p)k|^{\alpha(x_p)} - ikx_p], \quad (10)$$

with k the normalized wave number, $k = \bar{k}L$. The inverse Fourier transform of Eq. (10) gives a distribution with a peak value at $x = x_p$, $L_{\text{pdf}}\{[\alpha(x_p), \gamma(x_p)], x - x_p\}$.

III. CONSTRUCTING THE *M* MATRIX

The matrix, $\boldsymbol{M}'$, is a square matrix of size $(N + 1) \times (N + 1)$ and its construction is based upon a position vector with $N + 1$ points, with spacing $h = 1/N$. Each spatial location is denoted as $x_n = nh$, $n = 1, 2, 3, \ldots, N + 1$. The matrix operator, $\boldsymbol{M}'$, is constructed column by column because the parameter values of the jump pdf are constant for fixed column number. The values of the row elements of the matrix arise from the column construction procedure. The ith row in the matrix $\boldsymbol{M}'$ when multiplied by the profile column vector, $\boldsymbol{T}$, represents the integral operator terms [two terms on the left-hand side of Eq. (6)] evaluated at the location x_i. Each spatial location along the position vector is represented by the diagonal element of the square matrix $\boldsymbol{M}'$. For the ith row, each element of the row can be thought of as representing the integration variable x_{ij}, with i fixed and j ranging from 1 to N. The product of the ith row of $\boldsymbol{M}'$ with the column vector

$\boldsymbol{T}$ is assigned to the position x_i. Each member of the set of parameters $[\alpha, \gamma]$, characterizing the Lévy jump distribution can be either constant or vary with position. For the case of constant parameters $[\alpha, \gamma]$, the jump distributions at every x position vary only as regards their proximity to the ends of the system and the effects of top hat truncation arising from the finite length of the system. For spatially varying parameters, the jump-distribution parameters vary with column number; that is, they are a function of the integration variable x'_{ij}. In general, columns and rows are different for $\boldsymbol{M}'$ matrices (even with constant parameter values), but this difference is rectified when the matrix is explicitly made self-adjoint.

The details of the construction of the self-adjoint matrix, $\boldsymbol{M}$, are as follows. The ith row of the matrix $\boldsymbol{m}$ as given in Eq. (7) consists of the elements of an integral convolution, of the jump distribution, and the T profile. The $\boldsymbol{m}$ matrix, whose elements are denoted by m_{ij}, is created, column by column, by computing a Lévy α-stable distribution with parameters $[\alpha(x_j), \gamma(x_j)]$ by the inverse Fourier transform of the Lévy characteristic function given in Eq. (10). The columns of the matrix are computed since the jump pdf parameters are constant for fixed column number j. The peak of the distributions are at $x_j = x_i$, that is, along the diagonal. The rows of the $\boldsymbol{m}$ matrix arise naturally from the column-filling procedure. The jump distributions used in this investigation are truncated by multiplication by a top hat function [refer to Eq. (3)]. The end limits of the nonlocal system at $x = 0$ and $x = 1$ provide a natural top hat truncation to the Lévy distributions. The columns containing the truncated distributions are then renormalized, so that $\sum_i f_{th}(x_i)m_{ij} = 1$, $\forall j$ [refer to Eq. (4)].

The rows of the $\boldsymbol{m}$ matrix generally do not satisfy the same unity sum condition as the columns because of the truncation process. This situation is rectified by making the $\boldsymbol{m}$ matrix self-adjoint, and then requiring "detailed balance" at each point, x_j. By "detailed balance" it is meant that the number of particles jumping to the point x_j from $x_i \neq x_j$ is equal to the number of particles jumping from x_j to the other points in the system for both rows and columns. Physically, this procedure prevents the generation of fictitious sources or sinks resulting from the spatial nonuniformity of the parameters.

Detailed balance is achieved by forming a self-adjoint operator, $\boldsymbol{M}$, from $\boldsymbol{M}' = \boldsymbol{I} - \boldsymbol{m}$. By the column construction process just described, it is assured that $\boldsymbol{C}_1\boldsymbol{M}' = -C_1\sum_{i=1}^{N} m_{ij} + C_1 = 0$, with $\boldsymbol{C}_1$ a constant row vector (i.e., all elements have the same numerical value). This relation results from having normalized the truncated Lévy distributions along the columns of $\boldsymbol{m}$ to unity during construction of the $\boldsymbol{m}$ matrix. The transpose of the $\boldsymbol{M}'$ operator does not generally satisfy the detailed balance condition, and the product $\boldsymbol{M}'\boldsymbol{C}_1^{\dagger} = \boldsymbol{C}_1\boldsymbol{M}'^{\dagger} \neq 0$ (the "dagger" symbol denotes the transpose operation). Detailed balance can be achieved by subtracting a diagonal matrix, $\boldsymbol{M}_{\text{diag}}(\boldsymbol{R}_c)$, from the self-adjoint form of $\boldsymbol{m}$, $\boldsymbol{m}_{\text{SA}} = \frac{1}{2}(\boldsymbol{m} + \boldsymbol{m}^{\dagger})$. The row vector, $\boldsymbol{R}_c$, is the product of the self-adjoint form of $\boldsymbol{m}$ with the unit element column vector, $\boldsymbol{I}_c$, $\boldsymbol{R}_c = \boldsymbol{m}_{\text{SA}}\boldsymbol{I}_c$. To be clear, $\boldsymbol{I}_c$ is the column vector of length $N + 1$ with all elements equal to 1. The ith element of the vector $\boldsymbol{R}_c$ thus contains the integration (summation) of the ith row of the matrix $\boldsymbol{m}_{\text{SA}}$. The

self-adjoint matrix that satisfies the detailed balance condition with spatially varying jump-distribution parameters is, then,

$$M = M_{\text{diag}}(R_c) - m_{\text{SA}} \rightarrow I - \bar{m}_{\text{SA}}. \quad (11)$$

The term $M_{\text{diag}}(R_c)$ indicates the $(N + 1) \times (N + 1)$ matrix with the vector, R_c, along the diagonal. In order that each row and column of the matrix m_{SA} represents a probability density function, it is modified so that the sum of each row (and thus also the corresponding column) is unity. Using the modified matrix $\bar{m}_{\text{SA}}$ in place of m_{SA} then gives a $M_{\text{diag}}(R_c)$ matrix that is the identity matrix [the second form of M in Eq. (11)]. The use of the $M_{\text{diag}}(R_c)$ technique may therefore seem unnecessary, but it proves useful for forming the matrix bounded by material walls (Appendix C). The form of the matrix operator, M, given in Eq. (11) is self-adjoint, and by construction satisfies the detailed balance condition, $M I_c = I_c^{\dagger} M^{\dagger} = 0$. This condition ensures that the integral (sum in discretized form) of all rows and all columns is zero. Detailed balance, in the steady state with no source term [$S(x) = 0$], means that all of the jumps out of position x to other positions x', are balanced by jumps into position x from other positions, x', ensuring that the constant vector C_1 does not change, with time, at x. When a source is present, detailed balance ensures that the total flux out of the system is equal to the source flux. That is, the self-adjoint matrix operator does not contain spurious sources or sinks.

IV. STEADY-STATE BEHAVIOR

The steady-state (i.e., time-independent) behavior is described by Eq. (9) with the temporal derivative set to zero and M' replaced by M,

$$MT = S. \quad (12)$$

The matrix operator, M, is computed numerically at discrete points on a "calculation grid." The calculation grid is set out along the position variable (x axis) at $N + 1$ evenly spaced locations (N intervals). The distance between points is denoted by h with $h = 1/N$. The grid spacing, h, is dimensionless because the position variable has been normalized to the system length, $x = \bar{x}/L$. An important question is the choice of the number of grid points, N. The key considerations in making this choice are the source scale length L_S, and the jump-distribution width γ. At a minimum, it is required that the calculation grid resolve variations in the source, $h = 1/N \leqslant L_S/L$. Subtle issues regarding the choice of grid size are presented in Appendix A for $\alpha \neq 2$, and for the special case of $\alpha = 2$ in Appendix B. It is shown in Appendix D that the grid spacing must satisfy the condition $\gamma \geqslant h$ in order to obtain the desired transport scaling.

A. Bounding walls

Many physical systems have bounding walls that are part of the transport environment. For the case of heat transport, the role of the material walls at the ends of the system can be modeled as standard heat conductors or insulators. Walls suitable for a system describing density transport would have different properties [e.g., emissive (recycling) or absorbent] and such walls are not considered in this study. Heat transport within conducting walls is local, and the associated

transport is represented by the second derivative operator. To incorporate heat-conducting material walls into the transport matrix representing the complete system, the elements of the transport operator M near the ends of the system are modified to have the form of a second derivative operator. The walls are added to the ends of the system and increase its overall length. The length of the nonlocal system remains L, and the position vector is normalized to the length of the nonlocal system, not the total length of the system, which is greater than L due to the added wall material.

Top hat truncation of the jump distributions occurs at the ends of the nonlocal system. Boundary conditions for the entire system are set at the outer limits of the material walls. Neumann or Dirichlet conditions are set at the first and last rows of the M operator by the usual techniques. Specifically, all elements of the first and last row are set to zero except for the diagonal element for Dirichlet conditions (function value), or the diagonal and neighboring element for Neumann conditions (function derivative).

The extended transport matrix has a range of grid points at both ends of the system, where the matrix rows have the form of a second derivative operator, $-\tau \bar{\kappa} \frac{\partial^2}{\partial^2 \bar{x}} T = -(\tau \bar{\kappa}/L^2) \frac{\partial^2}{\partial^2 x} T = -\kappa' \frac{\partial^2}{\partial^2 x} T$, with $\bar{\kappa}$ the heat transport coefficient of the wall material in physical units, κ' is the normalized heat transport coefficient, and x is the normalized position. In matrix form, the second derivative matrix operator has rows with the pattern $[-1, 2, -1]/h^2$, where 2 is the diagonal element. The M matrix is actually not explicitly dependent upon the parameter h, because the integral (sum) of each matrix row is normalized to unity. That is, the term $h\bar{\eta}[p(x_j), x_i - x_j]$ appearing in Eq. (7) is normalized by the term $\sum_j h\bar{\eta}[p(x_j), x_i - x_j]$, so that the explicit h dependence is eliminated. With this normalization, the matrix rows representing material walls should have the form $[-1, 2, -1]$ rather than $[-1, 2, -1]/h^2$. The model wall conductivity, κ, is thus related to the normalized conductivity κ', as

$$\kappa' = h^2 \kappa. \quad (13)$$

This relationship is useful when comparing calculations performed on grids of different size.

In the language of the jump distribution, in which information is communicated by jumps between grid points, the second derivative operator communicates information only between neighboring grid points. That is, all jumps in the wall material are of length h, and jumps from a grid location can only occur to the left or right neighbor. In contrast, jumps in the nonlocal system can occur between grid locations many grid steps, h, apart. The property of localized, or one-step jumps in the wall material, is used to interface the wall with the nonlocal system.

Fuzzy wall

The nonlocal system and material walls have very different characteristics, and it is important to achieve a suitable match between the two. This requirement is accomplished by employing an interface between the two systems referred to as a "fuzzy wall." For reasons discussed in Appendixes A, B, and D, the relationship between the jump-distribution width γ, and the grid spacing h, is restricted to the regime $\gamma \geqslant h$. With this restriction in mind, the fuzzy wall is defined as a region
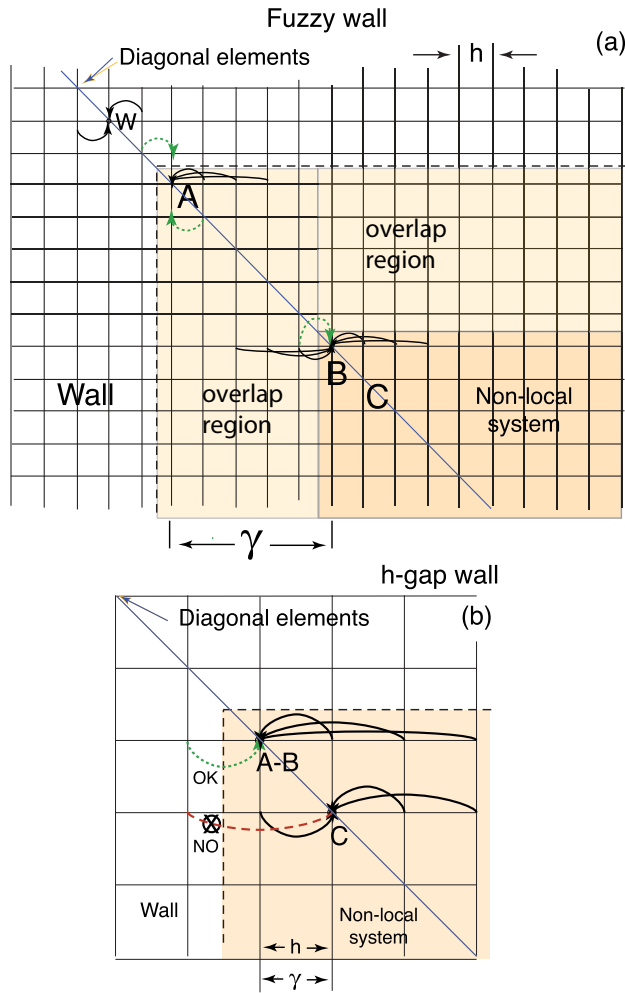
FIG. 1. (a) The fuzzy wall is an overlap region, one gamma in width, between the material wall (not shaded) and nonlocal system (shaded). Point A has both right and left jumps from the material wall. Point B has only a right jump from the wall, but both right and left jumps from the nonlocal system. (b) The minimum-width fuzzy wall, or h-gap wall occurs in the case $\gamma = h$. Points A and B in panel (a) coalesce to the point A-B. Arches denote jumps connecting row elements. Only wall jumps to point A-B in the nonlocal system are permitted (dotted green arch). Point C is too far from the wall (two grid points) to receive jumps from the wall material (dashed red arch).

of overlap between the wall material and the nonlocal system that is one jump-distribution width, γ, in size. Therefore, the width of the overlap region associated with the fuzzy wall is always greater than or equal to one grid spacing, h. If the ratio γ/h is not an integer then the integer part of this ratio is used to determine the number of grid points in the fuzzy wall.

The region of overlap between the wall and nonlocal system in the fuzzy wall concept is illustrated in Fig. 1(a). The nonlocal system and overlap region are shaded, and the wall region is unshaded. The physical interface between the wall and the system is indicated by the dashed black line. The computation grid is situated so that grid points are located, either entirely in the nonlocal system, or entirely within the wall, but not along the wall-system interface. The diagonal elements of the transport matrix (solid magenta diagonal line) represent

spatial locations, x, in the system and the other grid points in each individual row (that is, for fixed row number—horizontal line in the figure) represent the integration variable, x', of the integral operator formulation [refer to Eq. (7)]. The transport matrix is self-adjoint and thus there are equal overlap regions for both columns and rows. The form of the convolution integral in Eq. (7) corresponds to jumps along a matrix row, so that process is discussed in detail here. For fixed row number, the jumps associated with the jump-distribution calculation occur between row elements. For example, the grid point marked "W" in Fig. 1(a) is a spatial location in the wall that is adjacent to the nonlocal system. The solid black "arches" along the grid row containing the point W, represent jumps from the two neighboring grid points to the point W and are analogous to jumps associated with the jump distribution technique used to construct the nonlocal matrix $\boldsymbol{m}$. In the construction of the $\boldsymbol{m}$ matrix using a jump distribution, jumps are from a row position x' to the diagonal element x, from both the left and right. Jumps do not cross, or jump over, the diagonal element.

The interface between the left wall and nonlocal system is illustrated, but a similar situation is encountered at the interface at the right wall. The overlap region is limited in extent to one jump-distribution width γ, and extends from point A up to, but not including, point B shown in Fig. 1(a). Point A is the last point in the nonlocal system, and the truncation of the jump distributions occurs at this location. Point B marks the location of the final diagonal element connected to the wall material, and point C is the first spatial location not connected to the wall. Point B is connected to the wall by a single jump from the left (dotted green arch). All other locations in the fuzzy wall have jumps from the wall to the diagonal elements from both the left and right. Point A, however, only receives nonlocal system jumps from the right.

In the fuzzy wall region, the wall material is extended into the nonlocal system to create the overlap region. The truncated jump distributions are not changed between points A and B by the extended wall material. All jump distributions are truncated on the left at point A, as if the wall material in the overlap region were absent. Similarly the wall parameters are not changed in the overlap region (kappa remains the same). The overlap occurs without alteration to either system; the matrix rows for each system are simply added together in the overlap region. The parameter values, in the left and right walls, may be different depending upon the spatial variation of the parameters between the walls.

Figure 1(b) illustrates the minimum fuzzy wall configuration, which occurs in the case that $\gamma = h$. This particular configuration is referred to as the h-gap wall and it provides a detailed view of the elements of the fuzzy wall. The point marked A in Fig. 1(a) coalesces with point B and is marked A-B in Fig. 1(b). A-B marks the first spatial point (diagonal element) in the nonlocal system. Point A-B is located one grid spacing, h, from the material wall and, thus, this configuration is referred to as the "h-gap" wall. Jumps, in the nonlocal system, from all other grid points in the row containing point A-B, are connected to the point A-B. The nonlocal jumps come to point A-B from the right, and are indicated by the solid black arches to the right of point A-B, along the row containing A-B. For clarity, only three grid points in the nonlocal system are shown, but in a typical calculation there would be many more

grid points. Since point A-B is located only one grid spacing from the wall, jumps from the wall to point A-B are permitted, as indicated by the dotted green arch marked by "OK." This is the channel through which the wall and system exchange information. The spatial point denoted by "C" is located two grid spaces from the wall and jumps from the wall to point C are not permitted, as indicated by the dashed red arch marked by "NO." In contrast to the general fuzzy wall configuration, only point A-B communicates information to and from the wall in the h-gap configuration.

The use of the fuzzy wall is illustrated later by concrete examples. The details for constructing the transport matrix M_w, which represents a nonlocal system bounded on either end by material walls, are presented in Appendix C.

B. Convective term

The jump distributions, used in the construction of the matrix m, are truncated at the material walls surrounding the nonlocal system. In the truncation process, nonlocal jumps, that would occur from row locations that correspond to the material wall, are not allowed, and the jump distribution is set to zero at these locations. Since the jump distribution represents a probability distribution, the truncated distribution is renormalized, so that its spatial integral (sum) is unity. Thus, the truncation process leads to asymmetric jump distributions in the vicinity of the material walls. The degree of asymmetry depends upon the alpha value and width of the jump distribution. Jump distributions in the center of the system are symmetric and have zero first moment. Distributions near the walls have nonzero first moments. The first moment of the distribution can be considered to represent a "velocity" or "flow" and result in transport that is analogous to the process of "convection." Thus the M operator is considered to contain, at least partially, a "convective" operator of the form $\mathrm{v}_c \frac{\partial}{\partial x}$. The velocity $\mathbf{v}_c$ is a column vector equal to the first moment of matrix $\bar{m}_{\mathrm{SA}}$,

$$\mathrm{v}_c(\alpha, i) = h \sum_{j=1}^{N+1} (\bar{m}_{\mathrm{SA}})_{ij} \cdot (x_i - x_j). \tag{14}$$

In computing the first moment, only matrix elements representing the nonlocal system are included, i.e., the matrix $\bar{m}_{\mathrm{SA}}$, since this is the matrix containing the truncated jump distributions. The truncation points are located at the ends of the nonlocal system so that the flow is computed only for the nonlocal system. The flow in the wall material is assumed to be zero. If gamma is larger than the grid spacing h, the overlap region in the fuzzy wall does not affect the first moment calculation. A convective operator matrix M_1 is formed from the velocity vector $\mathrm{v}_c(\alpha, i)$, computed using Eq. (14), and defined as $M_1 = M_{\mathrm{diag}}[\mathbf{v}_c(\alpha)]D_1$. The matrix D_1 is the first derivative operator, a bidiagonal matrix with all rows except the first and last rows of the nonlocal system, having row elements $[-1/2h, 0, 1/2h]$, with 0 the diagonal element. The first row of the nonlocal system has the form $[-1/h, 1/h]$, with $-1/h$ the diagonal element. The last row of the nonlocal system has the same form, but with $1/h$ the diagonal element.

With the explicit dependence of the first moment $\mathbf{v}_c$ on grid spacing h, as indicated in Eq. (14), and with the first derivative operator proportional to $1/h$, the convective operator M_1 does

not explicitly depend upon the calculation grid spacing h. This independence from grid parameter h is the same as for the "total" matrix operator for a system bounded by material walls, M_w, and the two operators can be added or subtracted to form a new h-independent operator, M_2, that does not include the effects of convection,

$$M_2 = M_w - M_1 = M_w - M_{\mathrm{diag}}[\mathbf{v}_c(\alpha)]D_1. \tag{15}$$

The model systems examined in this study are bounded by material walls that can only conduct heat. Although it is easy enough to add a convective term to the model wall, this possibility is not included in this study. No heat convection (material flow) explicitly occurs in the walls. The flows associated with the convective velocity term given in Eq. (14) are entirely contained within the nonlocal system. That is, the first moment is nonzero only at points within the nonlocal system. It is instructive, at times, to investigate the difference between the transport matrix with and without the convective term. However, the flow terms are an important part of nonlocal transport and the convective term should always be included in the transport matrix when making a comparison to experimental data.

C. Spatial profiles

Steady-state profiles that satisfy Eq. (12) are determined, not only by the values of $[\alpha, \gamma]$ but also by the wall conductivity κ. To gain an understanding of the effect of variations in these basic quantities, several steady-state profiles are numerically evaluated for various parameter settings in the same model system. The model system consists of a nonlocal region bounded on both sides with walls of equal length and conductivity. The calculation grid consists of 1201 points, 100 grid points for each wall and 1001 grid points in the nonlocal system. The grid spacing is $h = 0.001$. The source is either symmetric about the center, or centrally located, with Gaussian spatial shape and scale length $\sigma = 0.005 = 5h$. The variation with alpha, at fixed gamma and kappa, is explored first and then alpha and kappa are held constant while gamma is varied. Finally the variation with kappa is investigated with fixed alpha and gamma values.

1. Dependence on alpha

Figure 2 shows spatial profiles of the scalar quantity T for three values of alpha, $\alpha = 1.4$, 1.8, and 2, with $[\gamma, \kappa] = [h, 1]$. All profiles are obtained with Dirichlet boundary conditions set at the ends of the system; the profile is zero at both ends. Figure 2(a) shows profiles associated with two equal sources located equidistant from the system center at $x = 0.35$ and $x = 0.65$ ($x = 0$ corresponds to the interface between the left wall and nonlocal system). The "flatter" profiles associated with lower values of alpha, indicate that transport increases with decreasing alpha, as expected. The profiles show a "hollow" profile phenomenon in that the value of the profile in the region between the two sources is less than at the source. This behavior is in contrast with the $\alpha = 2$ case in which the profile is flat (constant value) between the sources. The hollow profile effect arises from the tails of the Lévy jump distributions and increases with decreasing alpha.
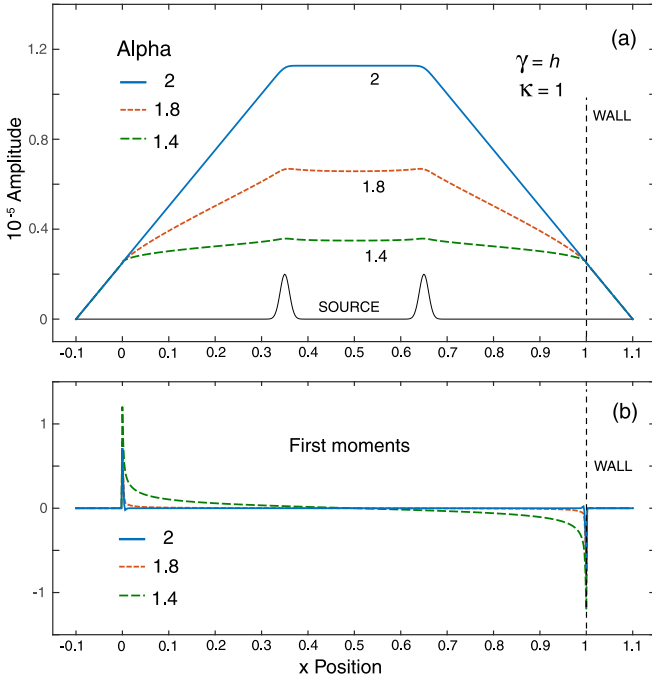
FIG. 2. (a) Steady-state profiles for three alpha values and $[\gamma, \kappa] = [h, 1]$ for two sources symmetrically located about the center position. The profile for $\alpha = 2$ is flat between the two sources, but the profiles for the other alpha values exhibit hollow profiles. That is, the central regions of the profiles are lower in amplitude than the amplitude at the source. (b) The first moments (multiplied by 10^3) are a matrix property and do not depend upon source location. The first moment becomes dominant as the alpha value nears unity.

Such an effect has been identified previously in a study of nonlocal transport based on fractional diffusion [21].

The first moments computed using Eq. (14) are shown in Fig. 2(b). The first moment term is antisymmetric (relative to the center of the nonlocal system) and the convection associated with the first moment is inward toward the center of the nonlocal system. As the value of alpha decreases, both the magnitudes of the first moments, and penetration into the nonlocal part of the system (extent away from the walls) increase. The first moment is the dominant feature of transport at alpha values near unity. The first moment is a property of the transport matrix and is not dependent upon source location, or the conductivity of the walls.

2. Dependence on gamma

Figure 3 illustrates the necessity of employing a technique such as the fuzzy wall. The case of $\gamma = \bar{\gamma}/L = 0.01$ is presented, employing two calculation grids, one with 121 points and thus $\gamma = h$, and the other with 1201 grid points so that $\gamma = 10h$. In the latter case two calculations are presented; one with an h-gap wall (dashed green curve), and the other with a fuzzy wall (orange curve with star symbols). The value of alpha is $\alpha = 1.5$, but the value of kappa depends upon the number of grid points. For the case with $N = 121$, kappa is chosen to have the value $\kappa' = \kappa = 1$, so that for $N = 1201$, using Eq. (13) and keeping κ' constant, $\kappa = 100$, since $(h_{1201}/h_{121})^2 = 0.01$. With the fuzzy wall, the calculation with
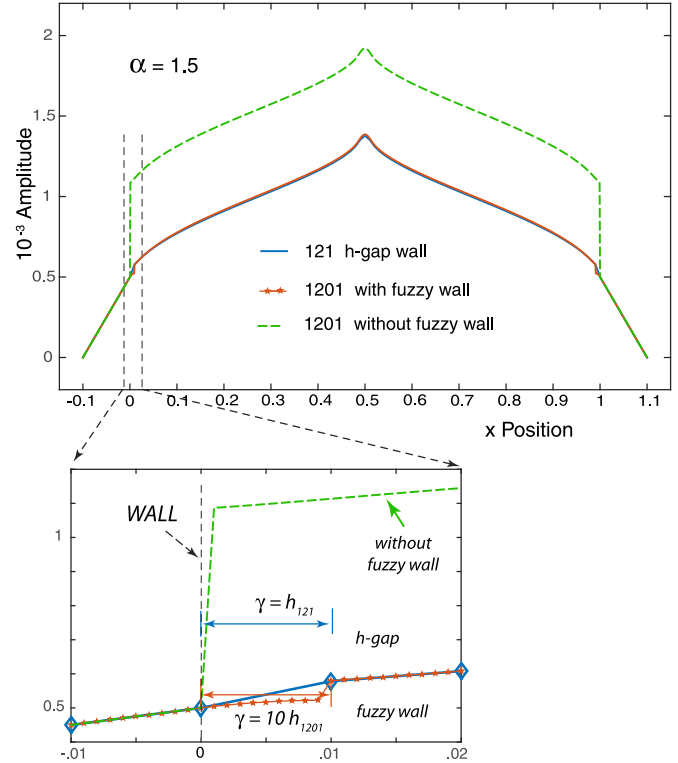

FIG. 3. Profiles obtained for fixed $\gamma = 0.01$, computed using two calculation grids, $N = 121$ and 1201, are compared. The profile computed without using a fuzzy wall (dashed green curve) exhibits a jump between the wall and nonlocal system. The profile computed using a fuzzy wall, $\gamma = 10h$, $N = 1201$ (orange curve with star symbols), agrees with the profile computed with an h-gap wall, $\gamma = h$, $N = 121$ (solid blue curve).

the smaller number of grid points and $\gamma = h$ (solid blue curve), produces the same profile as the $\gamma = 10h$ calculation using a fuzzy wall (orange curve with star symbols). The $\gamma = 10h$ case computed using a minimum-gap wall (h-gap wall) instead of a fuzzy wall, produces a profile with a jump between the wall-connected row and the first row entirely within the nonlocal system. The profile shape within the nonlocal system is the same in both $\gamma = 10h$ cases, except for the jump. In the case of an h-gap wall, the jump becomes larger for the same value of γ as the number of grid points increases. Therefore, for the h-gap wall, the calculation of the profile does not converge as N increases and $h \to 0$. In contrast, the use of a fuzzy wall yields profiles that remain the same as N increases, and it is this behavior that justifies the use of the fuzzy wall concept.

Figure 4 shows the effects of changing jump-distribution width γ on the steady-state profiles. The alpha and kappa values are the same for all profiles, $[\alpha, \kappa] = [1.5, 10]$. The calculation grid has $N = 1201$, and the source is centrally located. Four values of gamma, $\gamma = \bar{\gamma}/L = 0.001$, 0.002, 0.004, 0.008, corresponding to $h, 2h, 4h,$ and $8h$, are used for illustration. It is clear that transport increases with increasing gamma. The change in transport coefficient is quantified in Appendix D. The first moments, shown in Fig. 4(b), increase with increasing gamma, and they have a broader extent, that is, extend farther into the system, as the value of gamma increases.
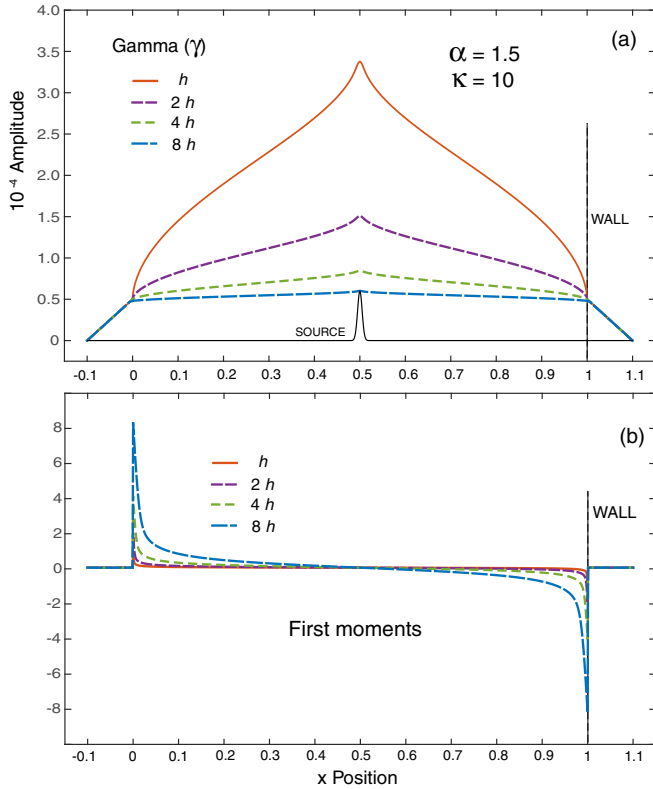
FIG. 4. (a) Steady-state profiles for fixed alpha and kappa are shown for changing jump-distribution width. The source is centrally located and the profiles become flatter with increasing gamma. (b) The first moments (multiplied by 10^3) for the gamma values used in (a) become larger as gamma increases.

3. Kappa dependence

Figure 5 illustrates the effects of changing the normalized wall conductivity, κ, on the steady-state profiles. The first moments for all the profiles shown in this figure are the same. That is, the first moment is not affected by the changing value of kappa. The first moment for the profiles shown in Fig. 5 is the same as the trace shown in Fig. 4(b) for the case $\gamma = h$(solid orange curve). The wall conductivity ranges from 0.5 to 100. The lower end of the conductivity range represents kappa values smaller than the transport coefficient in the nonlocal system, and the walls are "insulating" relative to the interior. Higher values of kappa represent walls that are more "conducting" than the interior system. The profiles inside the nonlocal system are identical in shape; the value of kappa simply determines the value of the profile at the wall. The value of the profile at the wall is set by the condition that the flux at the beginning of the wall is equal to the flux provided by the source. Since the system is symmetric, the source flux to the left wall is $S/2$ and the thermal flux in the wall $\kappa \partial T/\partial x \approx \kappa T_{\text{wall}}/x_{\text{wall}}$ must equal $S/2$, so that $T_{\text{wall}} = 0.5 S x_{\text{wall}}/\kappa$, and the larger kappa is, the smaller T_{wall} is.

D. Spatially varying parameters

The steady-state profile resulting from a spatial variation in the jump-distribution order parameter α is shown in Fig. 6. In Fig. 6(a), the alpha parameter has the value 2 in the center
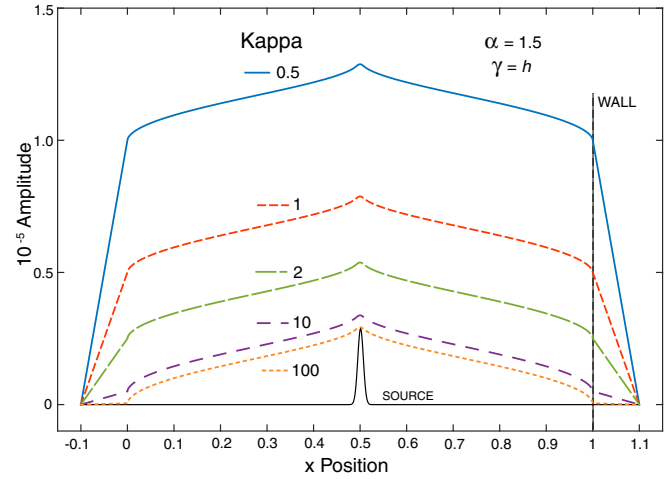

FIG. 5. Profiles for fixed nonlocal system parameters $[\alpha, \gamma] = [1.5, h]$ for different kappa values ranging from 0.5 to 100. Low values of kappa are insulating, and high values conducting, relative to the nonlocal system. The profile shape within the nonlocal system is invariant, and the effect of changing kappa value is to change the amplitude value at the wall-system interface.
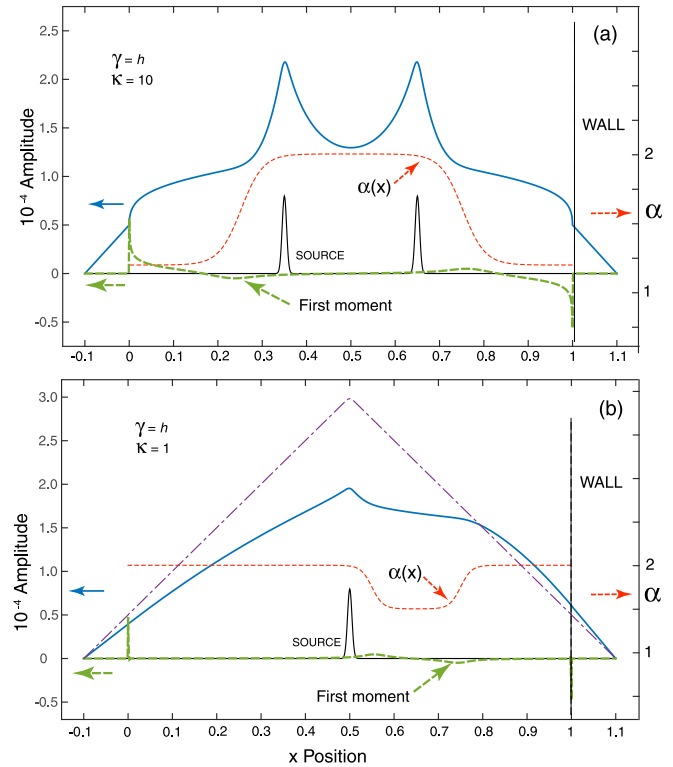

FIG. 6. Effect of spatially varying alpha parameter. (a) The value of alpha (dotted red curve) changes from 2 in the center of the system to 1.2 near the walls. The other parameters are $[\gamma, \kappa] = [h, 10]$. (b) The alpha parameter (dotted red curve) changes from 2 to 1.5 in a localized, off-center region to the right of center. The other parameters are $[\gamma, \kappa] = [h, 1]$. The dash-dot magenta curve shows the profile associated with a spatially uniform value of alpha, $\alpha = 2$. The first moments (dashed green curves) exhibit regions of internal flows produced by the gradients in alpha parameter in addition to the flows near the walls.

of the system, and gradually decreases to 1.2 near the ends of the system (dotted red curve, right-hand scale). This system has approximately "standard" transport in the center, in that the alpha value is 2, and becomes very nonlocal near the walls, where the alpha value is 1.2. The width of the jump distributions in both cases is $\gamma = h = 0.001$, and $\kappa = 10$. The source is the same as in Fig. 2 consisting of two Gaussians of width 0.005 with centers located at $x = 0.35$ and 0.65. The nonlocality of the distributions near the walls results in a central hollow profile, as compared to the constant profile associated with a uniform $\alpha = 2$ case [refer to Fig. 2(a)]. The hollow profile associated with spatially varying alpha is much more evident than for a spatially constant value of alpha less than 2 [refer to Fig. 2(a)]. The hollow profile effect is due to the tails of the Lévy distributions in the $\alpha = 1.2$ regions on the outer edges reaching across the entire system. The profile (solid blue curve) changes rapidly near the wall, due to the substantial increase of the magnitude of the first moment near the wall (dashed green curve).

Figure 6(b) shows another example of spatially varying alpha, but in this case the variation is not symmetric. The value of alpha is 2 except for a region on the right of the system where it drops in value to 1.5. This limited region of nonlocal behavior affects the entire profile. It results in an asymmetric profile (solid blue curve) in which the flux to the left wall is less than the flux to the right wall even though the source is centrally located. The dash-dot magenta line shows the profile shape that would result if alpha had a spatially uniform value of 2. Note that, for both profiles, the first moments (dashed green curves) show flows generated in the regions of the alpha gradients. The flows are opposite the direction of the alpha gradient and the flow is localized to the alpha gradient region.

Figure 7 shows the effects of spatial variation in the jump-distribution width for a fixed value of alpha, $\alpha = 1.2$. The jump-distribution width decreases from $4h$ near the walls to h in the middle (dotted red curve, right-hand scale) for a change of a factor of about 5.3 $[(4h/h)^{1.2} = 5.278]$ in the transport coefficient. The profile (solid blue curve) associated with this parameter variation is morphologically similar to the profile for changing alpha value shown in Fig. 6(a), in that transport is larger on the outside of the nonlocal system
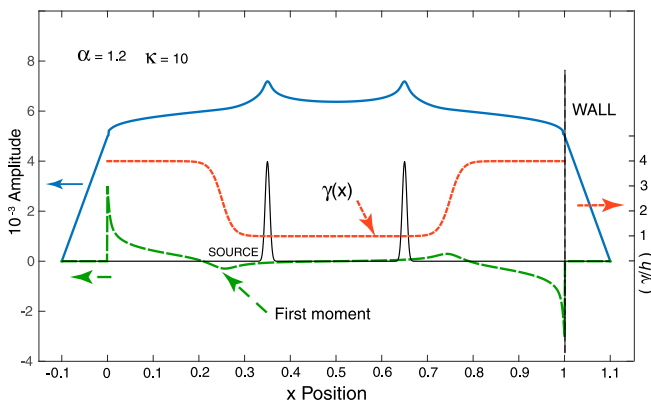

FIG. 7. An example of spatial variation in the jump-distribution width, gamma, for fixed alpha value, $\alpha = 1.2$. The value of gamma changes from $4h$ near the walls to h in the center of the system. The result is a very flat profile (solid blue curve).

as compared to transport in the central region. The most noticeable differences are that the first moment (dashed green curve) is much larger near the wall region and the profile is quite flat due to the increase in the transport coefficient on the outside of the system. Note that the gradient in the distribution width also results in flows generated in the gradient region of the width parameter. In contrast to the alpha gradient case, the flow is in the same direction of the gradient in gamma. Again, like the alpha gradient generated flow, the gamma gradient generated flow is localized to the gradient region.

V. TIME DEPENDENCE

An illustration of the versatility of the integral operator approach to studies of nonlocal transport properties is given by a time-dependent example. Time-dependent features (e.g., heat pulses) for situations in which the Lévy distributions remain temporally constant can be investigated by using Eq. (9),

$$\frac{\partial}{\partial t}\boldsymbol{T}_n(t) + \boldsymbol{M}_w \boldsymbol{T}_n(t) = \boldsymbol{S}_n(t), \qquad (16)$$

with $\boldsymbol{T}_n(t)$ denoting the discrete spatial profile as a function of time, $\boldsymbol{T}_n(t) = \boldsymbol{T}(nx, t)$, and, where t is normalized to the waiting time, τ, $t = \bar{t}/\tau$. With the time also a discrete vector, Eq. (16) becomes

$$\frac{\boldsymbol{T}^{m+1} - \boldsymbol{T}^m}{\Delta t} = -\boldsymbol{M}_w[a\boldsymbol{T}^{m+1} + (1-a)\boldsymbol{T}^m]$$
$$+ a\boldsymbol{S}^{m+1} + (1-a)\boldsymbol{S}^m, \qquad (17)$$

where Δt is the time step and the spatial subscript is dropped for economy of notation, $\boldsymbol{T}^m = \boldsymbol{T}(m\Delta t)$. The constant a is used to provide numerical stability, and for the examples shown here, a is adjusted with changing alpha parameter, $a = (3 - \alpha)/2$. For situations in which alpha is spatially varying, a spatially averaged value of alpha is used to evaluate a. Multiplying Eq. (17) by $\boldsymbol{M}_w^{-1}$ and solving for $\boldsymbol{T}^{m+1}$ gives

$$\boldsymbol{T}^{m+1} = \left[a\boldsymbol{I} + \frac{\boldsymbol{M}_w^{-1}}{\Delta t}\right]^{-1}\left\{\left[-(1-a)\boldsymbol{I} + \frac{\boldsymbol{M}_w^{-1}}{\Delta t}\right]\boldsymbol{T}^m\right.$$
$$\left. + \boldsymbol{M}_w^{-1}\bar{\boldsymbol{S}}^m\right\}, \qquad (18)$$

where $\bar{\boldsymbol{S}}^m = a\boldsymbol{S}^{m+1} + (1-a)\boldsymbol{S}^m$ and $\boldsymbol{I}$ is the identity matrix.

An example of the use of Eq. (18) to solve a time-dependent problem is given for a system with two constant (time-independent), Gaussian profile sources located at $x = 0.35$ and $x = 0.65$. The model system has a nonlocal region 1001 grid points in length, bounded by walls 100 grid points in width, and with wall conductivity $\kappa = 10$. A time-dependent problem is produced by introducing into this system a sink with a Gaussian spatial profile five grid points wide ($\sigma_{\text{sink}} = 0.005$) centered at $x = 0.15$, and with a Gaussian-shaped, temporal-pulse behavior, $S_{cp}(t) = \exp\{-[(t - 3000)/1000]^2\}$. The time vector is 401 points in length and $0 \leqslant t \leqslant 2 \times 10^4$. The time variation of the sink is chosen to obtain pulse propagation into the nonlocal system for the spatially uniform value of alpha ($\alpha = 1.2$) chosen for the example shown in Fig. 9(a). The system response to a spatially localized pulse of fixed temporal length varies considerably with alpha value. The fixed-length
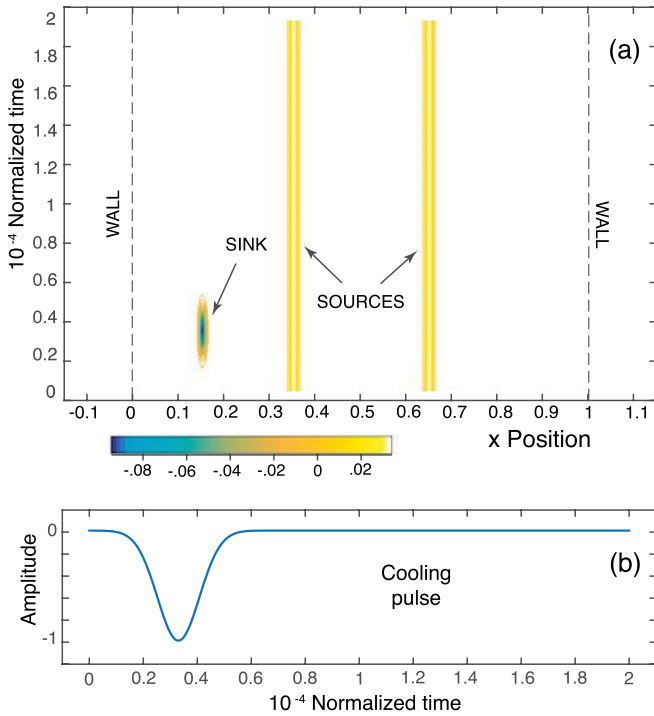
FIG. 8. (a) Contours of the source-sink combination used in the time-dependent examples shown in Figs. 9 and 10. (b) The time dependence of the amplitude of the cooling pulse.

pulse generates shorter wavelengths for larger alpha values. For the time-dependent examples, the full transport matrix (i.e., with the convective term included) is used to compute profiles. A contour plot of the source-sink combination is shown in Fig. 8(a) as a function of normalized position and normalized time. The pulse amplitude as a function of normalized time is shown in Fig. 8(b) over the entire time interval displayed in the contour plots shown in Figs. 9 and 10.

The solution to Eq. (18) with a constant alpha value, $\alpha = 1.2$, and a constant jump-distribution width, $\gamma = h$, is shown as a contour plot in Fig. 9(a). What is displayed is the difference between the system with the cooling pulse present and the system without the pulse. The time step used to obtain the solutions is $\Delta t = 50$.

The results do not change if the time step is set to a smaller value. The contour plots display the entire time interval spanned in Fig. 8(b), even though the pulse duration is only a small part. It is clear from the shape of the contours (constant amplitude lines) that the cold pulse propagates into the nonlocal system. At late times, the entire nonlocal system responds as it recovers from the initial pulse. For the low value of alpha used in this example ($\alpha = 1.2$), the pulse propagates through the nonlocal system all the way to the opposite wall. This effect is a visible manifestation of the nonlocal nature of the system.

Figure 9(b) shows the cooling pulse in a nonlocal system with spatially varying gamma parameter as shown in Fig. 7. The gamma profile is shown as the dotted red trace in Fig. 7. Gamma changes from $\gamma = 4h$ on the outside to $\gamma = h$ in the center of the nonlocal system with alpha held constant at $\alpha = 1.2$. Figure 9(b) shows contours of the difference between
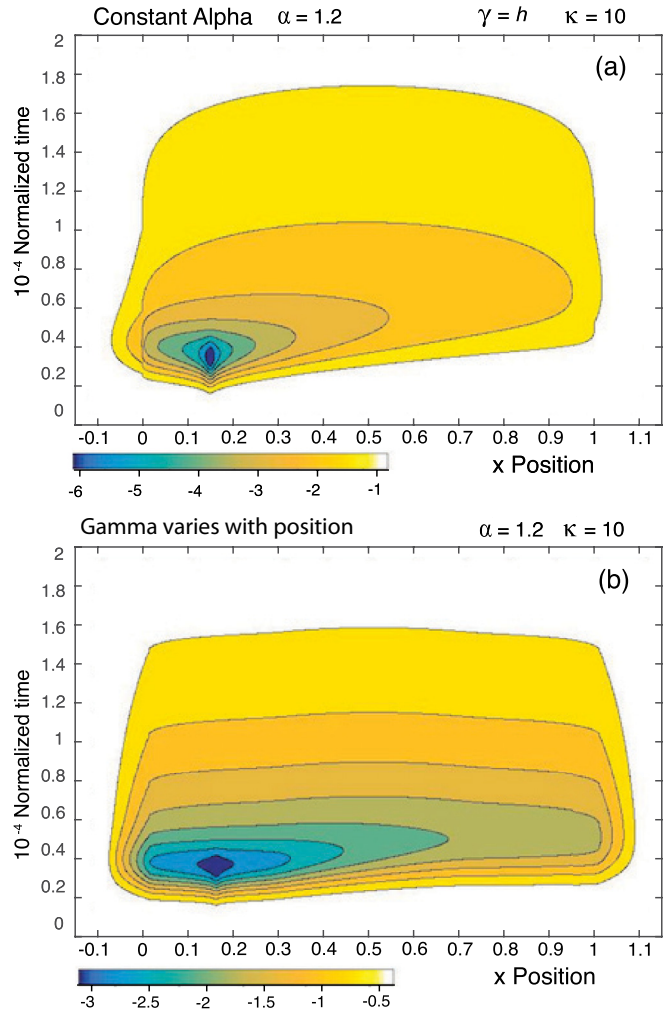

FIG. 9. (a). The effects of the cooling pulse in a system with constant gamma value, $\gamma = h$. (b) The cooling pulse in a system in which gamma varies from $4h$ on the outside to h in the center as in Fig. 7.
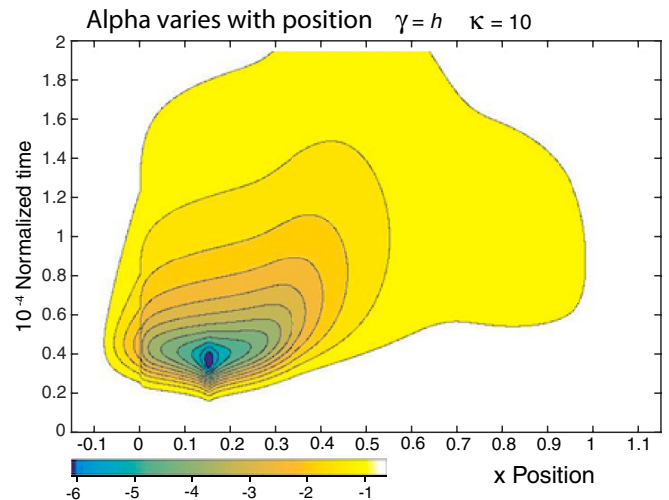

FIG. 10. Cooling pulse in a system with alpha varying from 1.2 on the outside to 2 in the middle, as in Fig. 6(a).

a system with the pulse present and a system without the pulse. The source-sink combination is the same as used in the constant gamma case shown in Fig. 9(a). In this example the cooling pulse moves rapidly across the nonlocal system to the opposite wall. The response to the cooling pulse propagates almost like a "plane" wave in the nonlocal system with very flat contours (constant amplitude lines). The large gamma value on the outer edges of the nonlocal system serves to strongly tie the two walls together.

Figure 10 shows contours of cooling-pulse propagation in a system in which the parameter alpha changes from a value of 1.2 on the outside to a value of 2 in the center. The spatial profile of the parameter alpha is shown as the dotted red trace in Fig. 6(a). The jump-distribution width is held constant at $\gamma = h$. The source-sink combination is the same as used in the previous cases shown in Fig. 9. For this situation, the pulse propagates to the center of the system with a longer delay than the constant parameter case shown in Fig. 9(a). Pulse penetration to the other side of the system is weak and delayed compared to the constant parameter case. The $\alpha = 2$ core acts as a barrier between the sink and the far side of the system.

VI. DISCUSSION AND CONCLUSIONS

An integral operator approach to nonlocal transport in finite bounded systems has been developed. The model system is a nonlocal region bounded by material walls with standard diffusive transport. The method starts with a Markovian master equation that uses a jump distribution to describe the transport of a scalar quantity. The jump distributions used in this study are Lévy α-stable probability distribution functions. The walls of the bounded system provide a natural top hat truncation of the jump distributions that results in a convective transport term proportional to the first moment of the jump-distribution matrix. Convective flow due to truncation at the walls is always inward and thus represents a "pinch" of the nonlocal system.

The integral operator formulation in a discretized system results in matrices as a description of transport. Matrices representing nonlocal transport can be obtained for values of alpha, the order parameter of the Lévy α-stable distribution, varying continuously from 1 to 2. The two extremes of the alpha parameter range correspond to two well-known spatial probability distribution functions; the Gaussian distribution for $\alpha = 2$ and the Cauchy distribution for $\alpha = 1$. This correspondence allows the model to be compared to standard transport models. The integral operator with $\alpha = 2$ reduces to the tridiagonal representation of the second derivative operator used in modeling diffusive transport in the small γ limit.

Although not presented in the main body of this manuscript, a detailed study of the transport coefficient associated with the self-adjoint operator is presented in the Appendixes. For the special case of $\alpha = 2$, treated in Appendix B, the transport coefficient is proportional to the square of the jump-distribution width, γ^2, provided the calculation grid resolves the peak of the jump distribution ($\gamma/h \geqslant 1$). In the opposite limit, $\gamma/h < 1$, the matrix is tridiagonal, but the scaling changes. The scaling of profiles for alpha values other than 2 is discussed in Appendix D, and it is demonstrated that profiles obtained using a transport matrix, with the first moment removed, scale as $\gamma^{-\alpha}$ for $\gamma/h \geqslant 1$. The scaling for

profiles with alpha values other than 2 also changes when γ/h becomes small ($\gamma/h < 1$) from $\gamma^{-\alpha}$ to $\gamma^{-(\alpha+1)}$. The change in scaling leads to the imposition of the restriction that the calculation grid must be able to resolve the jump-distribution peak. That is, the ratio of distribution width to grid spacing must be larger than unity, $\gamma/h \geqslant 1$.

The nonlocal system with alpha values other than 2 is characterized by hollow profiles due to the tails of the Lévy jump distributions extending across the entire system. Even when the central region has an alpha value of 2, the profile is hollow if the outer regions are characterized by alpha values less than 2. Spatial variations in parameter values also have a strong effect on the propagation of heat pulses. Regions of nonlocality connect the distant walls of the system, resulting in localized heat pulses becoming global structures. In contrast, a central region of standard transport ($\alpha = 2$) can act as a barrier to pulse penetration. The time-dependent examples presented highlight the value of the capability, built into the formulation, to allow the jump-distribution parameters to vary with position. Internal flows are generated by gradients in the distribution parameters. Flows are opposite to the gradient direction for changes in alpha, and in the gradient direction for changes in gamma. Internal flows are localized to the region of parameter gradients.

The integral operator technique is very versatile and can be used to model nonuniform, nonlocal systems of broad interest. An illustration of this capability is presented in Fig. 11 in which the example of a composite material interface presented by Stickler and Schachinger [25] is solved using the integral operator method. The solid blue curve mimics the result in Fig. 3 of Ref. [25]; it is obtained by extending the left-hand wall, with a high kappa value, to cover half the system. The dashed red curve represents the behavior at an actual interface between two nonlocal systems. The parameters change abruptly in the middle of the system from alpha equal
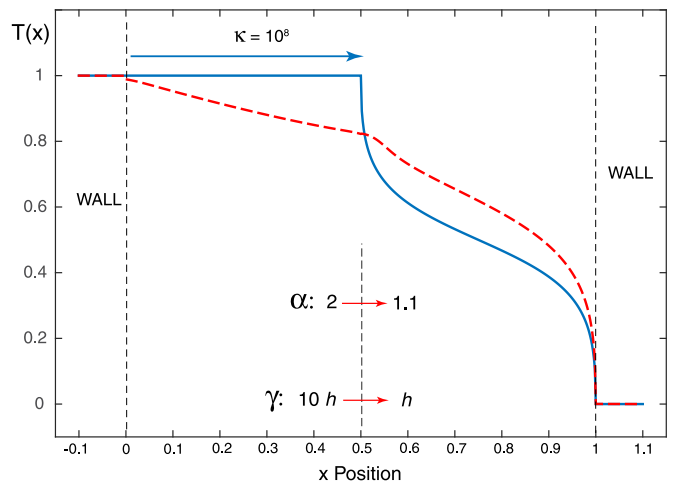

FIG. 11. The solid blue curve is a comparison to a case treated in Fig. 3 of Ref. [24]. To obtain the blue curve, the left-hand side of the system ($x < 0.5$) is wall material with $\kappa = 10^8$, and the right-hand side is a nonlocal system with $\alpha = 1.1$, $\gamma = 1$. The dashed red curve is obtained in a wall-to-wall nonlocal system with a step transition from $\alpha = 2$ to 1.1 in the center of the system, and a similar transition for γ from $10\,h$ to h.

to 2 to 1.1 and from gamma equal to $10h$ to h. The self-adjoint integral operator appropriately handles the interface between two nonlocal systems and the discontinuous derivative in the solid blue curve at the interface is resolved to a continuous change in the dashed red curve.

In using spatially nonuniform jump-distribution parameters it is essential that the transport matrix is self-adjoint. This property is necessary to avoid spurious sources and sinks arising from the spatial variation in parameters. The self-adjoint property of the matrices assures that the internal flows generated by gradients in the parameters of the Lévy α-stable jump distributions are not spurious artifacts.

ACKNOWLEDGMENT

APPENDIX A: GRID SIZE

The issue of a suitable choice of h for a given value of the distribution width γ requires careful consideration. For values of alpha different than 2 ($\alpha \neq 2$), the jump distributions have algebraically decaying tails (proportional to $|x|^{-(\alpha+1)}$), so that, in principle, the jump-distribution width could be very much smaller than h ($\gamma \ll h$). In that case, the matrix operator constructed from the jump distribution depends almost solely upon the asymptotic behavior of the distribution. Figure 12 illustrates the effects of the distribution width γ on the matrix operator for the case $\alpha = 1.5$. In Fig. 12 the calculation grid spacing h is held constant and three distribution widths are illustrated; $\gamma/h = 10, 1, 0.1$. The jump distributions for each case are computed at fine resolution, but the distributions used in constructing the $\boldsymbol{M}$ matrix are sampled at the grid spacing h, so any fine scale spatial resolution used in the numerical computation of the jump distribution is reduced to the grid spacing h. Figure 12(a) shows the logarithm of the Lévy α-stable probability distribution functions (pdfs) at points along the calculation grid in the vicinity of the diagonal element of a matrix row near the center of the system, for the three values of γ. The distribution for $\gamma = 10h$ appears flat, while the distribution for $\gamma = 0.1h$ is sharply peaked. The distribution with large gamma value is completely resolved by the calculation grid spacing and features near the peak of the distribution are retained. In contrast, only the asymptotic region of the narrow-width jump distribution is resolved by the grid spacing and details near the peak are lost as the value of γ/h is reduced. Figure 12(b) shows rows of the matrix operator $\boldsymbol{M}$, constructed from the Lévy distributions shown in panel (a). Figure 12(c) shows the ratio between the lower diagonal element and the diagonal element for several γ/h values ranging from 0.01 to 10. The change in the slope of the curve between large and small values of γ/h is evident. This change occurs because the jump distributions, projected upon the calculation grid, display purely asymptotic behavior when γ/h is small. The loss of "resolution" of the jump-distribution peak, when γ/h is small, results in a clear change in the nature of the transport represented by the $\boldsymbol{M}$ matrix. This is the regime of asymptotic behavior that is
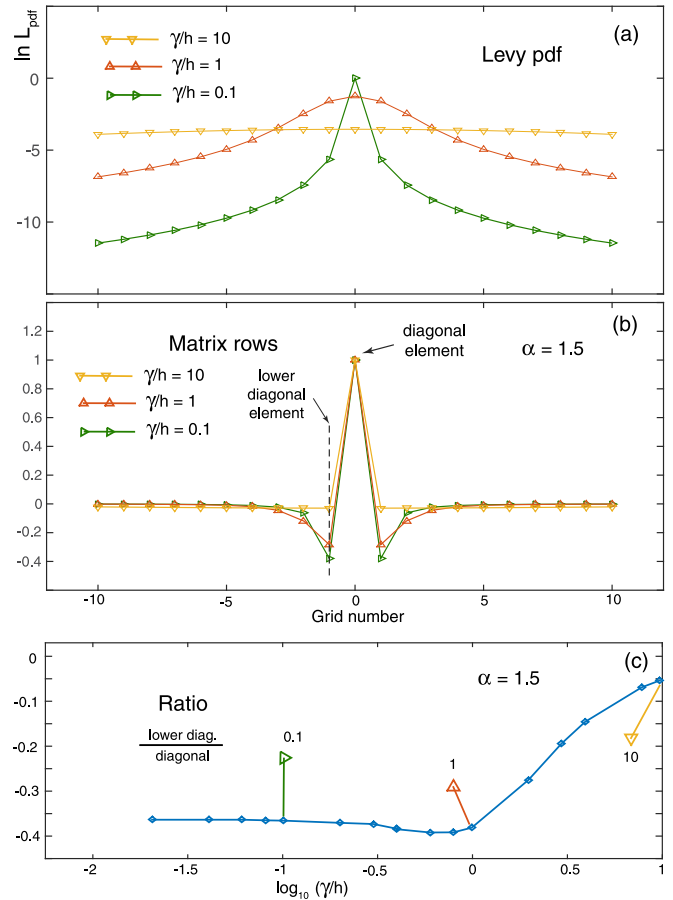

FIG. 12. (a) Logarithms of Lévy α-stable pdfs for three widths at constant grid spacing. (b) The matrix rows near the diagonal elements formed from each pdf. (c) The ratio of the lower diagonal element to the diagonal element for γ/h ratios ranging from 0.01 to 10. A clear change in behavior occurs for the transition $\gamma/h \gg 1$ to $\gamma/h \ll 1$.

sometimes represented by fractional derivative operators. In contrast to models that use only the asymptotic behavior of the Lévy pdf, the purely asymptotic regime is excluded in this study, and only calculation grids that resolve the peak of the jump distribution ($\gamma/h \gtrsim 1$) are used. Of course, the asymptotic parts of the jump distributions are retained, and play an important role in the present study.

APPENDIX B: $\alpha = 2$

The case with $\alpha = 2$ is special because the jump distributions do not have algebraic asymptotic behavior, but rather are exponentially decaying. The behavior of the $\boldsymbol{M}$ transport matrix as a function of γ/h must be considered separately. The relationship between the standard second derivative operator and the matrix operator with $\alpha = 2$ is

$$-\tau\chi\frac{\partial^2}{\partial^2\bar{x}} = -\chi'\frac{\partial^2}{\partial^2 x} = (\gamma/h)^2\boldsymbol{M}(2,\gamma), \qquad (B1)$$

where $\chi' = \tau\chi/L^2$ is the scaled transport coefficient. The second derivative operator is a tridiagonal matrix with each row having the form $[1, -2, 1]/h^2$ (-2 is the diagonal element). It is a fact that, over a limited range of γ values, $-\chi'\frac{\partial^2}{\partial^2 x}x^2 = -2\chi'$
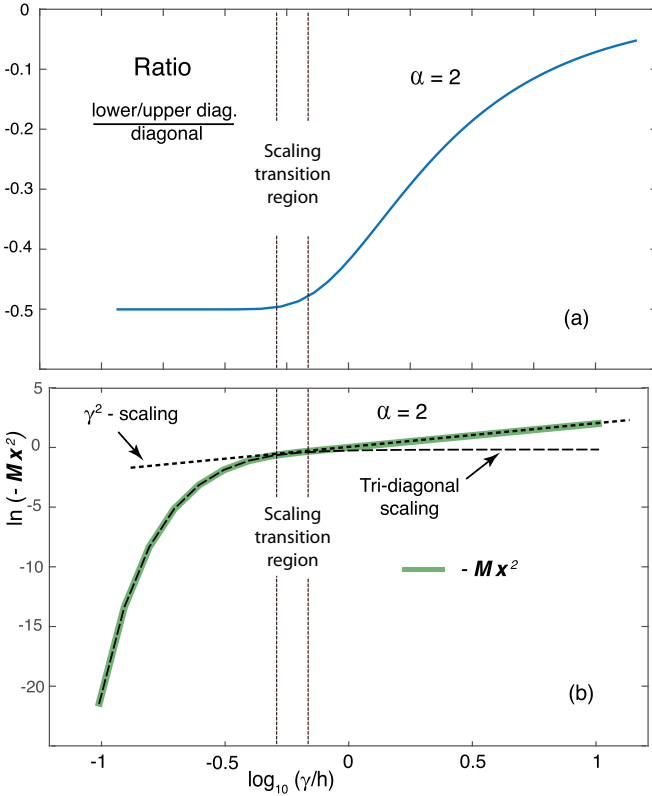
FIG. 13. The M operator achieves tridiagonal form at small γ/h values. (a) The ratio of lower and upper diagonal elements to the diagonal element goes to the value -0.5 for small γ/h, demonstrating that the matrix has tridiagonal form. (b) The scaling changes in the tridiagonal region (small γ/h).

and $(\gamma/h)^2 M(2,\gamma)x^2 = -2\gamma^2$, which indicates that $\chi' = \gamma^2$ in that range.

While the relation $M(2,\gamma)x^2 = -2\gamma^2$ holds over a limited range of γ/h, the question is, does the M operator with $\alpha = 2$ achieve the tridiagonal matrix form of the second derivative operator in the limit $\gamma/h \rightarrow 0$? For the tridiagonal second derivative matrix operator, the ratio of the upper and lower diagonal elements to the diagonal element is -0.5. Figure 13(a) shows that the M operator does achieve tridiagonal form in the limit $\gamma/h \rightarrow 0$ because the ratio of the upper and lower diagonal elements to the diagonal element is -0.5 when γ/h is small. Recall that the sum of any row of the M matrix is required to be zero. If the ratio of the lower and upper diagonal elements to the diagonal element is -0.5, it then follows that all other row elements are necessarily zero. Thus, the fact that the ratio of the lower diagonal and upper diagonal elements of the M matrix are -0.5 at small γ/h indicates that the form of the M matrix is indeed tridiagonal in this region. However, the scaling of the transport coefficient associated with the M matrix operator is not γ^2 in the limit $\gamma/h \rightarrow 0$.

In the limit $\gamma/h \rightarrow 0$, where the M matrix becomes tridiagonal in form, the scaling changes to the form given in Eq. (B2). With γ/h small, the elements of a row of the m matrix are reduced to three elements of measurably-nonzero amplitude, $[\Delta, 1, \Delta]/(1 + 2\Delta)$, where $\Delta = \exp(-h^2/\gamma^2) \ll 1$ and 1 is

the diagonal element. The other elements of the row are not strictly zero, but are too small to accurately calculate. The quantity $(1 + 2\Delta)$ normalizes the row so that the sum of the row elements is unity. In this limit the M matrix operating on x^2 becomes

$$
\begin{aligned}
Mx^2 = (I - m)x^2 &= \left\{ [0,\,1,\,0] - \frac{[\Delta,\,1,\,\Delta]}{(1+2\Delta)} \right\} x^2 \\
&= \frac{\Delta[-1,\,2,\,-1]}{1+2\Delta} x^2 = \frac{-2\Delta}{1+2\Delta}.
\end{aligned} \tag{B2}
$$

Figure 13 shows the quantity $-Mx^2$, the value of minus the M matrix operating on the square of the position column vector, x^2, as a function of γ/h. When γ/h is larger than unity, the γ^2 scaling prevails, but in the limit $\gamma/h \rightarrow 0$, the so-called "tridiagonal scaling" given by Eq. (B2) takes over.

APPENDIX C: DETAILS OF MATRIX CONSTRUCTION

The technique for constructing a transport matrix that represents a 1D nonlocal system bounded by material walls with transport coefficient κ is described in this Appendix. For simplicity, the situation in which the walls are of equal length and conductivity is considered, since the extension to the case of unequal wall length and different wall conductivities is straightforward. Let n_w denote the number of grid points in one wall, and denote the number of grid points in the nonlocal system by n_{sys}. This description pertains to the case of an h-gap wall, so that it is assumed $\gamma = h$ at the wall. The extension of the fuzzy wall technique used for larger values of gamma is again straightforward.

The matrix M_w describing transport in a nonlocal system bounded by material walls is constructed by first forming a square, bidiagonal matrix M_{bd} of size $n_{bd} = 2n_w + n_{\text{sys}}$, with rows of the form $[\kappa, 0, \kappa]$ (0 is the diagonal element). This form for the matrix elements may seem strange at first, but it will ultimately result in the wall rows having the form of a second derivative operator. The next step is to construct an m matrix of size $n_{\text{sys}} \times n_{\text{sys}}$ as described in Sec. III. The normalized, self-adjoint form of the matrix operator describing the jump distributions $\bar{m}_{\text{SA}}$ is then embedded into the bidiagonal matrix M_{bd}, using the prescription

$$
M_{bd}(n_w + 1:\, n_{bd} - n_w,\, n_w + 1:\, n_{bd} - n_w) = \bar{m}_{\text{SA}}. \tag{C1}
$$

With this embedding, the first and last n_w rows of M_{bd} represent material walls, and rows $n_w + 1$ to $n_w + n_{\text{sys}} + 1$ ($= n_{bd} - n_w$) represent the nonlocal system. The final transport matrix M_w is then

$$
M_w = M_{\text{diag}}(R_c) - M_{bd}. \tag{C2}
$$

Each element of the row vector R_c is obtained by multiplying each row of M_{bd} by the column vector C_1, which has all elements unity, $C_1(j) = 1, \forall j$. The row vector R_c has elements $R_c(i) = M_{bd}(i,\,:)C_1$. The notation $M_{\text{diag}}(R_c)$ denotes the square matrix whose diagonal elements are the vector R_c. With the final operation given in Eq. (C2), the rows representing the walls have the desired form: $[-\kappa,\, 2\kappa,\, -\kappa]$.

As a rule of thumb, values of kappa larger than unity, $\kappa > 1$, correspond to walls that are more conducting than the nonlocal system, while small values of kappa, $\kappa < 1$, correspond to

walls less conducting than the nonlocal system (i.e., insulating walls).

APPENDIX D: TRANSPORT SCALING

It is useful to establish the expected scaling of the transport coefficient with the parameter set $[\alpha, \gamma]$. Time integration of the Fourier transform of Eq. (1) gives

$$\ln[P(k, t)] = -t[1 - \tilde{\eta}(k)]. \tag{D1}$$

Using Eq. (10), the Fourier transform (characteristic function) of the Lévy distributions gives $\{1 - \tilde{\eta}([\alpha, \gamma], k)\} = (1 - e^{-\gamma^\alpha |k|^\alpha})$. In the small k limit, this expression is approximately $\gamma^\alpha |k|^\alpha$, and then Eq. (D1) can be approximated as

$$\ln[P(k, t)] = -t\gamma^\alpha |k|^\alpha; \quad |\gamma k| \ll 1. \tag{D2}$$

The standard diffusion equation in scaled variables ($\frac{\partial}{\partial t} P = D\frac{\partial^2}{\partial^2 x} P$) with constant diffusion coefficient D gives the relation $\ln[P(k, t)] = -Dk^2 t$, and using this relation in Eq. (D2) yields

$$\chi_\alpha \equiv \gamma^\alpha = D|k|^{2-\alpha}, \tag{D3}$$

where χ_α denotes the transport coefficient of the nonlocal system and is defined to be γ^α. All quantities in Eq. (D3) are scaled; $\gamma = \bar{\gamma}/L$; $D = \tau \bar{D}/L^2$; $k = \bar{k}L$ (the overbar denotes an unscaled quantity). Substituting the smallest value of k in the system into Eq. (D3), $k_{\text{cutoff}} \approx \pi$; $\bar{k}_{\text{cutoff}} = \pi/L$, gives an approximate relation between the nonlocal transport coefficient χ_α and the standard diffusion coefficient D,

$$\chi_\alpha = \gamma^\alpha = D\pi^{2-\alpha}, \tag{D4a}$$

$$\bar{\chi}_\alpha = \frac{\bar{\gamma}^\alpha}{\tau} = \bar{D}\left|\frac{L}{\pi}\right|^{\alpha-2}, \tag{D4b}$$

where Eq. (D4b) gives the same relation in unscaled quantities (physical units). The expression in Eq. (D4a) agrees with Eq. (B1), indicating that for $\alpha = 2$, χ_α is equal to D. For $\alpha = 1$, Eq. (D4b) agrees with the expression given by Vermeersch *et al.* [15] if their exponential cutoff variable, u_{BD}, is taken equal to the system length, $u_{BD} = L$. Equation (D4a) suggests that, for a fixed value of gamma, transport increases with decreasing alpha value (because $\gamma < 1$), and, for fixed alpha value, transport increases with increasing gamma.

Figure 14(a) shows a comparison between two profiles obtained with matrix operators constructed from jump distributions with widths $\gamma = h$ (solid red curve) and $\gamma = 3h$ (dashed blue curve), and with alpha value $\alpha = 1.2$. The amplitude of the profile with larger gamma value is smaller because the transport coefficient increases as gamma increases [Eq. (D4)]. The profiles shown in Fig. 14(a) are obtained with a matrix operator without the convective term included [M_2; refer to Eq. (15)]. The dotted black line indicates the profile obtained by multiplying the $\gamma = 3h$ profile by $(\gamma_1/\gamma_3)^{-\alpha} = (h/3h)^{-1.2} = 3.737$. These two profiles obtained with the M_2 operator follow $\gamma^{-\alpha}$ scaling. The dotted curve in Fig. 14(a) so closely follows the solid red curve that they are difficult to distinguish.

The results of a survey of profile scaling with the two jump-distribution parameters $[\alpha, \gamma]$ are shown in Fig. 14(b). The parameter survey is conducted using the technique presented
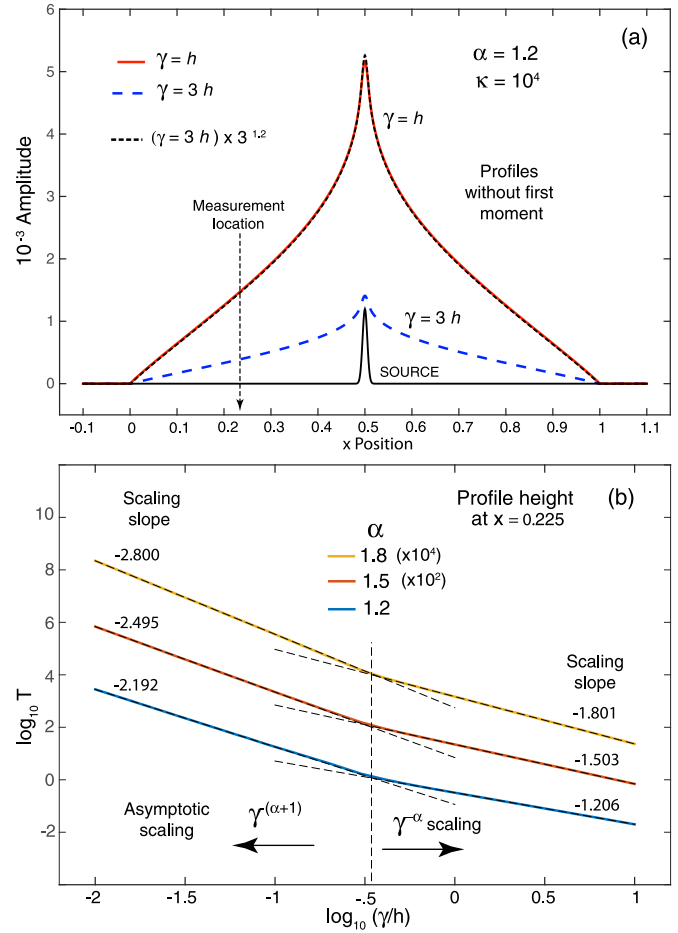

FIG. 14. (a) Profiles obtained without the convective term and with $\gamma \geqslant h$ do follow $\gamma^{-\alpha}$ scaling. The vertical dashed line indicates the location at which amplitude values are compared in the scaling survey shown in (b). (b) The scaling of profile amplitude with jump-distribution width is shown for three alpha values, 1.2, 1.5, and 1.8. Shown is the amplitude value (in logarithmic scale) of the profile at a fixed x location ($x = 0.225$) as gamma is varied by three orders of magnitude. Dashed lines are fits to the profile amplitude data. Scaling at small jump-distribution widths is dominated by the asymptotic scaling, $(\gamma/h)^{-(\alpha+1)}$, of the jump distributions.

in Fig. 14(a). Profiles are calculated using the M_2 operator, at a fixed alpha value, for a range of widths and then the amplitudes of the profiles are compared at a fixed x location ($x = 0.225$). The position at which the comparison is made in the parameter survey is shown in Fig. 14(a), and marked as "measurement location." The survey covers alpha values, $\alpha = 1.2$, 1.5, and 1.8, with gamma values in the range $0.01h \leqslant \gamma \leqslant 10h$. The traces are multiplied by 10^2 for $\alpha = 1.5$ and 10^4 for $\alpha = 1.8$, for clarity of display. Profiles are computed on a grid with $N = 4201$ and two walls with $n_w = 100$. Thus, in the computations, the value of h is fixed ($h = 2.5 \times 10^{-4}$), and the value of gamma is changed to vary the ratio γ/h. For each $[\alpha, \gamma]$ pair in the survey grid, a profile $T(x)$ is calculated using the M_2 matrix operator (no convective term) and the height of the profile at the point $x = 0.225$ is used as a representative value for the entire profile. The wall kappa value used in obtaining the profiles is $\kappa = 10^4$, so that none of the profile shapes are affected by the profile-wall boundary over the γ/h range

surveyed. The dashed lines shown in Fig. 14(b) are obtained by fitting the data, over the appropriate γ/h range, with a standard fitting routine (MATLAB *polyfit*).

Since, as illustrated in Fig. 14(a), profile amplitudes are smaller for larger gamma, the profile amplitude scales as the inverse of the transport coefficient. That is, for a system of fixed length and source, a larger transport coefficient results in a lower profile amplitude. For gamma values on the order of, or larger than, h ($\gamma \geqslant h$), the height of the profiles at a fixed point $x = 0.225$ scales as $\gamma^{-\alpha}$, that is, as the inverse of the transport

coefficient [refer to Eq. (D4a)]. For small values of gamma ($\gamma \leqslant 0.1h$), the profile height scales as the asymptotic algebraic decay of the jump distribution $(\gamma/h)^{-(\alpha+1)}$, quite distinct from the scaling at gamma values larger than h. This change in behavior is consistent with the change in the ratio of the lower diagonal element to the diagonal element of the matrix rows shown in Fig. 12. The asymptotic scaling range is not explored in this study. Calculation grids are chosen so that the peaks of the jump distributions are always resolved (i.e., $h \leqslant \gamma$).

[1] A. M. S. Mohammed, Y. R. Koh, B. Vermeersch, H. Lu, P. G. Burke, A. C. Gossard, and A. Shakouri, Nano Lett. **15**, 4269 (2015).

[2] S. Winnerl, F. Gottfert, M. Mittendorff, H. Schneider, M Helm, T. Winzer, E. Malic, A. Knorr, M. Orlita, M. Potemski, M. Sprinkle, C. Berger, and W. A. de Heer, J. Phys.: Condens. Matter **25**, 054202 (2013).

[3] U. Briskot, I. A. Dmitriev, and A. D. Mirlin, Phys. Rev. B **89**, 075414 (2014).

[4] K. T. Regner, D. P. Sellan, Z. Su, C. H. Amon, A. J. H. McGaughey, and J. A. Malen, Nat. Commun. **4**, 1640 (2013).

[5] K. W. Gentle, R. V. Bravenec, G. Cima, H. Gasquet, G. A. Hallock, P. E. Phillips, D. W. Ross, W. L. Rowan, A. J. Wootton, T. P. Crowley, J. Heard, A. Ouroua, P. M. Schoch, and C. Watts, Phys. Plasmas **2**, 2292 (1995).

[6] M. R. de Baar, M. N. A. Beurskens, G. M. D. Hogeweij, and N. J. L. Cardozo, Phys. Plasmas **6**, 4645 (1999).

[7] R. Jha, P. K. Kaw, D. R. Kulkarni, J. C. Parikh, and ADITYA Team, Phys. Plasmas **10**, 699 (2003).

[8] V. Gonchar, A. Chechkin, E. Sorokovoi, V. Chechkin, L. Grigoreva, and E. Volkov, Plasma Phys. Rep. **29**, 380 (2003).

[9] P. Mantica and F. Ryter, C. R. Phys. **7**, 634 (2006).

[10] P. Barthelemy, G. Bertolotti, and D. S. Wiersma, Nat. Lett. **453**, 495 (2008).

[11] V. Zaburdaev, S. Denisov, and J. Klaftr, Rev. Mod. Phys. **87**, 483 (2015).

[12] B. Dybiec, E. Gudowska-Nowak, and P. Hanggi, Phys. Rev. E **73**, 046104 (2006).

[13] C. De Mulatier, A. Rosso, and G. Schehr, J. Stat. Mech.: Theory Exp. (2013) P10006.

[14] R. N. Mantegna and H. E. Stanley, Phys. Rev. Lett. **73**, 2946 (1994).

[15] Á. Cartea and D. del-Castillo-Negrete, Phys. Rev. E **76**, 041105 (2007).

[16] B. Vermeersch, A. M. S. Mohammed, G. Pernot, Y. R. Koh, and A. Shakouri, Phys. Rev. B **91**, 085203 (2015).

[17] E. Montroll and G. H. Weiss, J. Math. Phys. **6**, 167 (1965).

[18] E. Montroll and Scher, J. Stat. Phys. **9**, 101 (1973).

[19] J. Klafter and R. Silbey, Phys. Rev. Lett. **44**, 55 (1980).

[20] J. Klafter, A. Blumen, and M. F. Shlesinger, Phys. Rev. A **35**, 3081 (1987).

[21] A. Kullberg, D. del-Castillo-Negrete, G. J. Morales, and J. E. Maggs, Phys. Rev. E **87**, 052115 (2013).

[22] A. Zoia, A. Rosso, and M. Kardar, Phys. Rev. E **76**, 021116 (2007).

[23] S. Lepri and A. Politi, Phys. Rev. E **83**, 030107 (2011).

[24] A. Kullberg, G. J. Morales, and J. E. Maggs, Phys. Plasmas **21**, 032310 (2014).

[25] B. A. Stickler and E. Schachinger, Phys. Rev. E **83**, 011122 (2011).

[26] G. Samorodnitsky and M. Taqqu, *Stable Non-Gaussian Random Processes: Stochastic Models with Infinite Variance* (CRC Press, New York, 1994).